

Hybrid Organic/Inorganic Band-Edge Modulation of *p*-Si(111) Photoelectrodes: Effects of R, Metal Oxide, and Pt on H₂ Generation

Junhyeok Seo,[‡] Hark Jin Kim,[‡] Ryan T. Pekarek, and Michael J. Rose*

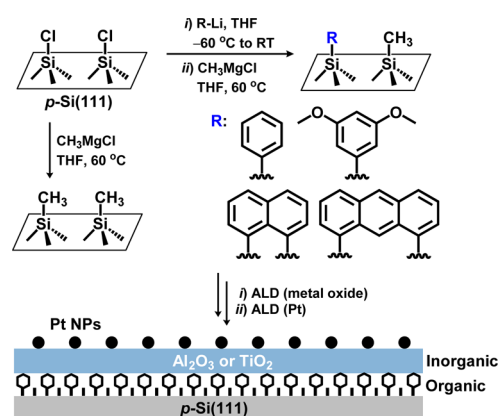
Department of Chemistry, The University of Texas at Austin, Austin, Texas 78712, United States

S Supporting Information

ABSTRACT: The efficient generation of dihydrogen on molecularly modified *p*-Si(111) has remained a challenge due to the low barrier heights observed on such surfaces. The band-edge and barrier height challenge is a primary obstruction to progress in the area of integration of molecular H₂ electrocatalysts with silicon photoelectrodes. In this work, we demonstrate that an optimal combination of organic passivating agent and inorganic metal oxide leads to H₂ evolution at photovoltages positive of RHE. Modulation of the passivating R group [CH₃ → Ph → Naph → Anth → Ph(OMe)₂] improves both the band-edge position and ΔV ($V_{\text{onset}} - V_{\text{max}}$). Subsequent atomic layer deposition (ALD) of Al₂O₃ or TiO₂ along with ALD-Pt deposition results in to our knowledge the first example of a positive H₂ operating potential on molecularly modified Si(111). Mott–Schottky analyses reveal that the flat-band potential of the stable Ph(OMe)₂ surface approaches that of the native (but unstable) hydride-terminated surface. The series resistance is diminished by the methoxy functional groups on the phenyl unit, due to its chemical and electronic connectivity with the TiO₂ layer. Overall, judicious choice of the R group in conjunction with TiO₂/Pt effects H₂ generation on *p*-Si(111) photoelectrodes ($V_{\text{oc}} = 207 \pm 5.2$ mV; $J_{\text{sc}} = -21.7$ mA/cm²; ff = 0.22; $\eta_{\text{H}_2} = 0.99\%$). These results provide a viable hybrid strategy toward the operation of catalysts on molecularly modified *p*-Si(111).

Integration of light absorbers with functional catalysts is one of the primary challenges in the area of solar fuels research.^{1–4} Silicon shows excellent potential as a putative light absorber in a parallel or tandem system,⁵ due to its ideal band gap ($E_g = 1.12$ eV) for the absorption of sunlight to drive the $2\text{H}^+ \rightarrow \text{H}_2$ conversion.⁶ In the arena of molecular catalysts, silicon also shows great promise because fully passivating coupling methods can be used to covalently attach catalysts to the surface.^{7–9} In this regime, the Si(111) surface presents one particular advantage over the Si(100) orientation used in most materials-based approaches: the upright orientation of Si-X bonds on Si(111) renders it uniquely suited for molecular modification. Its need for extreme bonding regularity (to prevent surface defect sites) can be fulfilled by molecular passivation—typically by methylation.¹⁰ Unfortunately, this process results in a negative dipole (−0.37 eV) and a corresponding low *p*-type barrier height.¹¹ Ultimately, this enforces a severe photocathodic shift in the band-edge

Scheme 1. Functionalization of *p*-Si(111)-Cl Substrates with -CH₃ or Aromatic Groups, Followed by Atomic Layer Deposition of a Metal Oxide and Pt



position (−0.5 to −0.3 V vs NHE), which renders such substrates untenable for efficient H₂ evolution.

In this work, we report a hybrid organic/inorganic approach to modulating the band-edge position of Si(111) substrates. Substitution of Si-CH₃ with aryl moieties modulates the band-edge by 50–300 mV, adjusting the operating potential of *p*-Si(111)|R|Pt devices closer to the H⁺/H₂ potential. An atomic layer deposition (ALD)-deposited metal oxide ultrathin film (~20 Å) serves as a protecting layer that further modulates the band-edge and serves as a reliable support for ALD-based Pt deposition. The identity of the metal oxide thin film (Al₂O₃, TiO₂) modulates the observed onset potentials. This hybrid molecular/materials approach leads to *p*-Si(111)|R|metal oxide|Pt photocathodes that operate well positive of the H⁺/H₂ potential under 1 sun illumination.

The two-step method of Si(111) functionalization reported by Lewis et al.¹² is employed to prepare chlorinated Si(111) substrates, which are subsequently treated with alkyl Grignard reagents (THF, 60 °C) or aryl lithium reagents (THF, −60 °C → RT) to afford the corresponding functionalized surfaces. A range of aryl reagents (Scheme 1) was investigated to determine the effect of the conjugated framework. A subsequent methylation step was used to fill-in any unpassivated Si-Cl sites, leading to highly stable surfaces that exhibit no observable SiO_x formation upon exposure to air.¹³

Received: December 12, 2014

Published: February 26, 2015

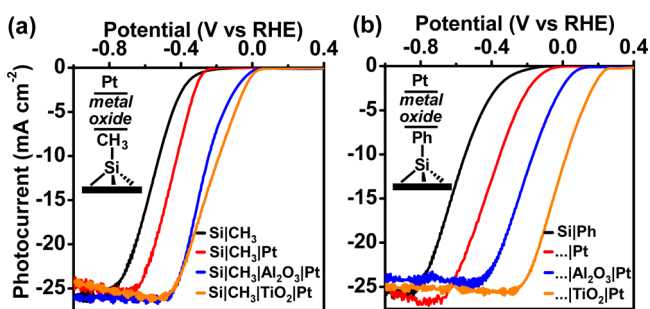


Figure 1. J - V curves of (a) p -Si(111)|CH₃ surfaces and (b) p -Si(111)|Ph surfaces: bare (black) and with ALD-Pt (red), Al₂O₃|Pt (blue), and TiO₂|Pt (orange). Conditions: 0.5 M H₂SO₄(aq), AM 1.5G 100 mW/cm², 0.1 V/s scan rate.

The J - V curve of p -Si(111)|CH₃ in aqueous 0.5 M H₂SO₄ (Figure 1a, black curve) reveals a very negative onset potential of -326 ± 3.7 mV vs RHE (where $V_{\text{onset}} = E$ for -1 mA/cm²). Such a negative onset potential is expected due to (i) the lack of a catalytic H⁺/H₂ species for H₂ evolution and (ii) the interfacial dipole of the Si-CH₃ surface.¹¹

We attempted to improve the performance of the Si-CH₃ substrate by adding catalytic Pt and a metal oxide.^{14–19} ALD-based deposition of Pt using [(MeCp)Pt(CH₃)₃] under mild conditions (O₂ pulse, 240 °C, 50 cycles) afforded a Pt-functionalized substrate. The resulting PEC-LSV (Figure 1a, red line) exhibited a nearly identical onset potential ($V_{\text{onset}} = -289 \pm 0.3$ mV) and slightly shifted light-limited photocurrent ($V_{j_{\text{max}}} = -672 \pm 3.5$ mV) as compared to the bare Si-CH₃ surface ($V_{\text{onset}} = -326 \pm 3.7$ mV; $V_{j_{\text{max}}} = -787 \pm 3.5$ mV). We next constructed a composite silmetal oxide device to provide a solid support for the Pt catalyst²⁰ and to modulate the onset potential of the device. Previously, the beneficial metal oxide effect has been attributed to the prevention of solution-mediated recombination at the substrate/electrolyte interface.¹⁶ An ultrathin layer of Al₂O₃ was deposited on the Si-CH₃ substrate by ALD (20 cycles of [Al(CH₃)₃]/H₂O, 150 °C; ~2 nm by XPS, see Supporting Information (SI)), followed by platinum ALD to generate Pt nanoparticles (NPs). The resulting PEC-LSV trace for the composite p -Si(111)|CH₃|Al₂O₃|Pt device (Figure 1a, blue) reveals a nearly +290 mV shift in onset potential, corresponding to $V_{\text{onset}} = -36 \pm 3.8$ mV vs RHE, ΔV ($V_{\text{onset}} - V_{j_{\text{max}}}$) = 421 ± 7.4 mV.

In a second test, an ultrathin film of TiO₂ was deposited on the Si-CH₃ substrate (50 cycles of [Ti(N(CH₃)₂)₄]/H₂O, 240 °C; ~2 nm by XPS, see SI). Pt NPs were then deposited by ALD (240 °C, 10 ± 2 nm by SEM; Figure S5, SI). Compared to Al₂O₃|Pt, the TiO₂|Pt modification provides a slightly improved onset potential (Figure 1a, orange; for TiO₂|Pt, $V_{\text{onset}} = -2 \pm 2.7$ mV vs RHE, $\Delta V = 406 \pm 5.1$ mV). Despite the different electronic properties of Al₂O₃ and crystalline TiO₂ (bandgap, band-edge, conductivity, etc.), the ultrathin (~2 nm) layer is too thin to emulate the bulk metal oxide and instead acts only as a tunneling barrier in the presence of Pt NPs (vide infra). Additionally, decreased surface recombination velocities (S , i.e., higher quality surfaces) are observed on the metal oxide|Pt deposited samples (Al₂O₃|Pt, $S = 1640$ cm/s; TiO₂|Pt, $S = 4690$ cm/s) as compared to the Pt-only deposited samples (7650 cm/s; Table S2, SI). It is also notable that the unmodified Si-H surface was severely oxidized during the TiO₂-ALD (Figure S2, SI), in contrast to the SiO_x-free samples protected with an organic monolayer. Surprisingly, the Al₂O₃-

ALD incurred a lesser extent of oxidation on the Si-H surface (Figure S2, SI), possibly due to adventitious methylation of Si-H by Al(CH₃)₃. Nonetheless, the performance of p -Si(111)|Hl Al₂O₃|Pt was poor ($V_{\text{onset}} \approx -0.5$ V; Figure S3, SI).

To better differentiate the effects of metal oxide and Pt, we carried out the same set of experiments with a phenyl-functionalized substrate. This substrate was prepared by treating Si(111)-Cl with phenyl lithium at -60 °C → RT, followed by passivation of remaining Si-Cl sites with CH₃MgCl in THF at 60 °C for 30 min. The resulting LSV (Figure 1b, black line) exhibits a slightly improved onset potential ($V_{\text{onset}} \approx -289 \pm 7.2$ mV vs RHE) but is still lower than that of a simple Pt wire electrode. However, the J - V curve following Pt deposition on the bare p -Si(111)-Ph device affords a significant anodic shift in the onset potential to -126 ± 3.1 mV vs RHE (Figure 1b, red). More importantly, deposition of Pt on the p -Si(111)|Ph|Al₂O₃ (Figure 1b, blue) and p -Si(111)|Ph|TiO₂ (orange) constructs affords a systematic increase of the onset potentials: $-289 \rightarrow -126 \rightarrow +44 \rightarrow +213$ mV vs RHE for the devices {bare} → {Pt} → {Al₂O₃|Pt} → {TiO₂|Pt}. The ΔV decreases in each case, e.g., $\Delta V = 501 \rightarrow 460$ mV for {Al₂O₃|Pt} → {TiO₂|Pt}. Ultimately, the phenyl-functionalized substrate p -Si(111)|Ph|TiO₂|Pt represents an improved H₂ photocathode ($V_{\text{onset}} = +213 \pm 9.7$ mV) compared to its methyl-functionalized congener p -Si(111)|CH₃|TiO₂|Pt ($V_{\text{onset}} = -2 \pm 2.7$ mV vs RHE).

Considering the favorable effect of the aromatic phenyl group, we elaborated the scope of aryl groups to include compounds with extended aromaticity, such as naphthalene (Naph) and anthracene (Anth). As such, 1,8-dibrominated Naph and Anth were di-lithiated with 1.8 equiv of n -BuLi in THF at -60 °C (Scheme 1) and then incubated with the Si(111)-Cl substrate from -60 °C → RT; any remaining Si-Cl sites were passivated with CH₃MgCl (THF, 60 °C). Ultra-high-resolution XPS analyses of the sp² sub-region (284.5 eV)²¹ of the C 1s features indicated surface coverages of 28% for Si-Ph, 17% for Si-Naph, and 8% for Si-Anth (Table S1, SI); these values represent the number of surface-attached organic moieties per atop Si site. Considering the increasing cross sections of Naph (6.46 Å) and Anth (8.95 Å) units [compared to Ph (4.05 Å)], the hydrocarbon coverages are likely equitable.

A comparison of the corresponding devices with formulation p -Si(111)|R|TiO₂|Pt (R = CH₃, Ph, Naph, Anth) is shown in Figure 2, and the performance parameters are given in Table 1. Inspection of the data reveals that the change from Ph → Naph → Anth gradually improved ΔV (Ph, 460 mV; Naph, 339 mV; Anth, 275 mV) and the potential of the light-limited, maximum photocurrent ($V_{j_{\text{max}}}$: Ph, -247 mV; Naph, -177 mV; Anth, =

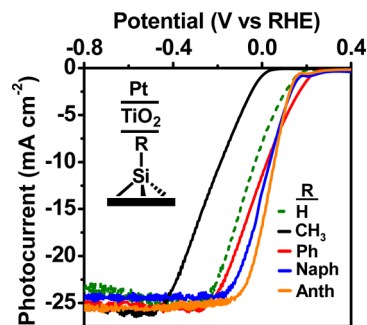


Figure 2. J - V curves of p -Si(111)|R|TiO₂|Pt for R = H, CH₃, Ph, Naph, and Anth. Conditions: 0.5 M H₂SO₄(aq), AM 1.5G 100 mW/cm², 0.1 V/s scan rate.

Table 1. Performance Parameters^a for Devices of Type *p*-Si(111)|R|TiO₂|Pt in 0.5 M H₂SO₄(aq) PEC-LSV Experiments

	R = CH ₃	R = Ph	R = Naph	R = Anth	R = diMeOPh	R = H
V_{onset}^b	-2 ± 2.7	213 ± 9.7	161 ± 4.9	148 ± 2.8	207 ± 5.2	192 ± 64
J_{max}^c	-26.7 ± 2.2	-25.3 ± 0.1	-24.2 ± 0.3	-24.8 ± 0.2	-25.0 ± 0.7	-25.1 ± 0.6
$V_{J_{\text{max}}}^d$	-407 ± 5.9	-247 ± 5.7	-177 ± 2.7	-127 ± 2.8	-81 ± 5.2	-247 ± 127
ΔV^e	406 ± 5.1	460 ± 4.3	339 ± 2.9	275 ± 0.5	288 ± 4.4	438 ± 78

^aAM 1.5G 100 mW/cm² illumination; experiments were performed in triplicate. Potentials in mV vs RHE. ^b V_{onset} was selected as the potential exhibiting -1 mA/cm² photocurrent density. ^c J_{max} (in mA/cm²) is the maximum light-limited photocurrent density. ^d $V_{J_{\text{max}}}$ is the potential at J_{max} .

$$^e \Delta V = V_{\text{onset}} - V_{J_{\text{max}}}$$

-127 mV). However, a slight decrease in the onset potential for H₂ catalysis is observed (V_{onset} : Ph, +213 mV; Anth, +148 mV).

To determine the origin of the increasingly efficient performance (and in an effort to effect further improvements), Mott–Schottky plots were generated for each “bare” *p*-Si(111)-R surface. It is important to note that a nearly ideal photocathode performance ($V_{\text{OC}} = +300$ mV vs RHE, $\eta = 2.1\%$) has been observed for *p*-Si(100)-H|Pt surfaces.²² However, these surfaces are extremely unstable in the absence of an applied cathodic potential and must be etched with HF prior to each set of linear sweep measurements. Thus, it is highly desirable to construct a device that has analogous metrics but exhibits air and aqueous stability. In our measurement, the performance of the simple *p*-Si(111)-H|TiO₂|Pt substrate was inferior to that of the aryl-modified substrates and was also very unreliable. The sample exhibited $V_{\text{onset}} = +192 \pm 64.3$ mV and $\Delta V = 438 \pm 77.8$ mV (Figure 2), where the positive V_{onset} , large ΔV , and high standard deviations were most likely due to uncontrolled oxidation processes during TiO₂-ALD (see the severely oxidized substrate, Figure S2, SI).

The Mott–Schottky behavior of a *p*-Si(111)-H substrate (Figure 3, green) exhibits the most positive flat-band potential,

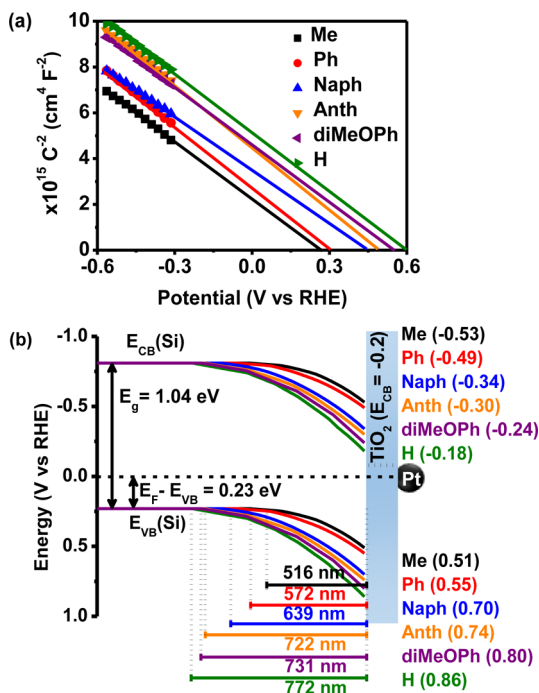


Figure 3. Mott–Schottky (a) and band-bending (b) plots of *p*-Si(111)-R substrates [R = H, CH₃, Ph, Naph, Anth, and 3,5-dimethoxyphenyl (diMeOPh)] to determine flat-band potential (E_{FB}). Conditions: 0.5 M H₂SO₄, dark, 10 kHz.

$E_{\text{FB}} = +630$ mV vs RHE in 0.5 M H₂SO₄(aq). In contrast, the methylated and phenyl-functionalized surfaces exhibit very low $E_{\text{FB}} = +280$ mV (CH₃, black) and +320 mV (Ph, red). While all of the Si surfaces modified with organic groups show comparable slopes (same carrier density), a trend of more positive E_{FB} potentials is observed in the order CH₃ → Ph → Naph → Anth. Accordingly, the depletion region (charged depth at the semiconductor/liquid junction) was extended in the same order. The metrics derived from Mott–Schottky analyses are summarized in a band-bending diagram (Figure 3b). Overall, it is notable that the surfaces presenting extended aromaticity exhibit E_{FB} values (Naph, +470 mV, blue; Anth, +510 mV, orange) approaching that of the ideal hydride surface (+630 mV).

Due to their ultrathin nature (~ 2 nm), the Al₂O₃ and TiO₂ layers act simply as a protective tunneling barrier through which electrons tunnel in the presence of Pt. From (i) the fact that Al₂O₃ does not impede electron transfer in the presence of Pt and (ii) the consistent positive shift in V_{onset} in Al₂O₃ vs TiO₂ samples, we conclude that the primary electronic effect of the metal oxide is to modulate the dipole¹¹ of the polarizable aryl units (note that the nonpolarizable -CH₃ shows the smallest effect). The ALD layers are too thin to act as “bulk” Al₂O₃ or TiO₂, wherein they would impose their formal band structure in matching the Si conduction band (CB) with the metal oxide CB.

Last, we utilized the modularity of the phenyl group to introduce dimethoxy functional groups in order to (i) modulate the electron density at the surface (to increase barrier height)²³ and (ii) promote a direct chemical interaction between the organic surface moiety and the inorganic TiO₂ layer. The resulting Mott–Schottky plot of the “bare” *p*-Si(111)|3,5-dimethoxyphenyl substrate (diMeOPh) exhibited a more positive potential than that of the *p*-Si(111)|Anth substrate (Figure 3a, violet). Additionally, the calculated charge depletion depth of Si(111)|diMeOPh (731 nm) was close to the ideal Si-H surface (772 nm).

Thus encouraged, we performed PEC-LSV with the composite *p*-Si(111)|diMeOPh|TiO₂|Pt device (Figure 4a). The experiment revealed a V_{onset} similar to that obtained with R = Ph but improved compared to R = Anth. Additionally, ΔV was significantly improved ($460 \rightarrow 288$ mV), corresponding to a sharper turn-on to maximum performance. This indicates that the series resistance (R_s) across the Si|TiO₂ interface was decreased in the presence of the methoxy group.²⁴ The organic oxygen moieties likely increase the chemical and electronic connectivity between bulk Si and the coordinative TiO₂ layer.²⁵ Electrochemical impedance spectroscopy revealed $R_s = 33.5 \Omega$ for the cell, and this was applied to compensate for the iR drop. Illumination of the sample at varying light intensities (0.5, 1, and 2 sun) generates the ideal, linearly modulated photocurrent densities ($-12.57 \rightarrow -24.69 \rightarrow -47.94$ mA/cm²) as expected for light-limiting conditions (Figure 4b). Not including the iR compensation, the voltammogram of *p*-Si(111)|diMeOPh|TiO₂|

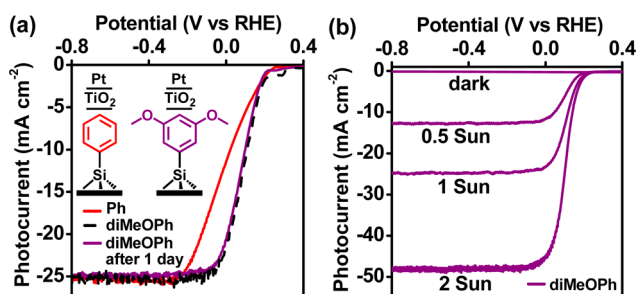


Figure 4. J - V curves for the optimized organic/inorganic photocathode: (a) p -Si(111)|Ph|TiO₂|Pt (red) and p -Si(111)|diMeOPh|TiO₂|Pt (violet) samples without iR compensation; (b) light dependence for p -Si(111)|diMeOPh|TiO₂|Pt with iR compensation. Conditions: 0.5 M H₂SO₄, AM 1.5G filter, $\nu = 0.1$ V/s, 100 mW/cm².

Pt (Figure 4a) revealed an improved fill factor ($ff = 0.22$), corresponding to a 0.99% solar-to-H₂ conversion efficiency (η_{H_2}). This is comparable to the efficiency parameters of known devices that require HF treatment before each use (p -Si-HIPt, $\eta_{H_2} = 1.1\%$)²⁶ but less than those derived from p/n^+ emitter buried junctions (p/n^+ -SiIPt, $\eta_{H_2} = 9.6\%$).²²

To test the stability of this optimized device, the rinsed substrate was stored for 24 h in ambient air conditions, and it exhibited no loss in performance metrics (Figure 4, dashed line). The stability of the device was further studied by chronoamperometry under continuous illumination at 0 V vs RHE for 90 h, where the performance of the device was limited only by the diminishing [H⁺] throughout the bulk electrophotolysis (Figure S7, SI). Thus, the composite p -Si(111)|diMeOPh|TiO₂|Pt device presents a set of new, stable benchmarks for H₂ evolution on molecularly modified p -Si(111).

In closing, we have demonstrated that a hybrid organic/inorganic functionalization scheme improves the performance of p -Si(111) photocathodes into the functional range. While judicious choice of organic functional group enhances the flat-band potential, a composite organic/metal oxide/Pt arrangement affords an efficient device. Additionally, more-direct chemical and electronic connectivity (introduction of an -OCH₃ intercalator) into the metal oxide layer diminishes the series resistance and provides the best performance. Such devices are air-stable under ambient air/light conditions and do not require re-etching with HF prior to re-use. Studies applying these principles to the attachment of earth-abundant molecular catalysts are underway.

■ ASSOCIATED CONTENT

Supporting Information

Procedures for Si etching, attachments, and ALD; XPS thickness measurements; PXRD for anatase TiO₂ and SEM for Pt NPs; extended data tables for PEC-LSV figures of merit; Mott-Schottky parameters; Tauc plot. This material is available free of charge via the Internet at <http://pubs.acs.org>.

■ AUTHOR INFORMATION

Corresponding Author

*mrose@cm.utexas.edu

Author Contributions

[‡]J.S. and H.J.K. contributed equally.

Notes

The authors declare no competing financial interest.

■ ACKNOWLEDGMENTS

This research was supported by the Office of Naval Research (N00014-13-10530), the Robert A. Welch Foundation (F-1822), and the ACS Petroleum Research Fund (53542-DN13). The authors gratefully acknowledge Dr. Hugo Celio for technical assistance with XPS measurements.

■ REFERENCES

- Modestino, M. A.; Walczak, K. A.; Berger, A.; Evans, C. M.; Haussener, S.; Koval, C.; Newman, J. S.; Ager, J. W.; Segalman, R. A. *Energy Environ. Sci.* **2014**, *7*, 297–301.
- Chen, X.; Shen, S.; Guo, L.; Mao, S. S. *Chem. Rev.* **2010**, *110*, 6503–6570.
- Reece, S. Y.; Hamel, J. A.; Sung, K.; Jarvi, T. D.; Esswein, A. J.; Pijpers, J. J. H.; Nocera, D. G. *Science* **2011**, *334*, 645–648.
- Rodriguez, C. A.; Modestino, M. A.; Psaltis, D.; Moser, C. *Energy Environ. Sci.* **2014**, *7*, 3828–3835.
- Hou, Y.; Abrams, B. L.; Vesborg, P. C. K.; Björketun, M. E.; Herbst, K.; Bech, L.; Setti, A. M.; Damsgaard, C. D.; Pedersen, T.; Hansen, O.; Rossmeisl, J.; Dahl, S.; Nørskov, J. K.; Chorkendorff, I. *Nat. Mater.* **2011**, *10*, 434–438.
- Walter, M. G.; Warren, E. L.; McKone, J. R.; Boettcher, S. W.; Mi, Q.; Santori, E. A.; Lewis, N. S. *Chem. Rev.* **2010**, *110*, 6446–6473.
- O’Leary, L. E.; Rose, M. J.; Ding, T. X.; Johansson, E.; Brunschwig, B. S.; Lewis, N. S. *J. Am. Chem. Soc.* **2013**, *135*, 10081–10090.
- Moore, G. F.; Sharp, I. D. *J. Phys. Chem. Lett.* **2013**, *4*, 568–572.
- Lattimer, J. R. C.; Blakemore, J. D.; Sattler, W.; Gul, S.; Chatterjee, R.; Yachandra, V. K.; Yano, J.; Brunschwig, B. S.; Lewis, N. S.; Gray, H. B. *Dalton Trans.* **2014**, *43*, 15004–15012.
- Wong, K. T.; Lewis, N. S. *Acc. Chem. Res.* **2014**, *47*, 3037–3044.
- (a) Grimm, R. L.; Bierman, M. J.; O’Leary, L. E.; Strandwitz, N. C.; Brunschwig, B. S.; Lewis, N. S. *J. Phys. Chem. C* **2012**, *116*, 23569–23576. (b) Gleason-Rohrer, D. C.; Brunschwig, B. S.; Lewis, N. S. *J. Phys. Chem. C* **2013**, *117*, 18031–18042.
- Bansal, A.; Li, X.; Lauermann, I.; Lewis, N. S.; Yi, S. L.; Weinberg, W. H. *J. Am. Chem. Soc.* **1996**, *118*, 7225–7226.
- Bansal, A.; Lewis, N. S. *J. Phys. Chem. B* **1998**, *102*, 4058–4060.
- Dasgupta, N. P.; Liu, C.; Andrews, S.; Prinz, F. B.; Yang, P. *J. Am. Chem. Soc.* **2013**, *135*, 12932–12935.
- Seger, B.; Pedersen, T.; Laursen, A. B.; Vesborg, P. C. K.; Hansen, O.; Chorkendorff, I. *J. Am. Chem. Soc.* **2013**, *135*, 1057–1064.
- Eisenberg, D.; Ahn, H. S.; Bard, A. J. *J. Am. Chem. Soc.* **2014**, *136*, 14011–14014.
- Hanson, K.; Losego, M. D.; Kalanyan, B.; Parsons, G. N.; Meyer, T. J. *Nano Lett.* **2013**, *13*, 4802–4809.
- Lin, Y.; Battaglia, C.; Boccard, M.; Hettick, M.; Yu, Z.; Ballif, C.; Ager, J. W.; Javey, A. *Nano Lett.* **2013**, *13*, 5615–5618.
- Hämäläinen, J.; Puukilainen, E.; Sajavaara, T.; Ritala, M.; Leskelä, M. *Thin Solid Films* **2013**, *531*, 243–250.
- Gaspard, P.; Hithesh, K. G.; Göran, S.; van der Wouter, W.; Niclas, R. *Nanotechnology* **2013**, *24*, 015602.
- Díaz, J.; Paolicelli, G.; Ferrer, S.; Comin, F. *Phys. Rev. B* **1996**, *54*, 8064–8069.
- Boettcher, S. W.; Warren, E. L.; Putnam, M. C.; Santori, E. A.; Turner-Evans, D.; Kelzenberg, M. D.; Walter, M. G.; McKone, J. R.; Brunschwig, B. S.; Atwater, H. A.; Lewis, N. S. *J. Am. Chem. Soc.* **2011**, *133*, 1216–1219.
- Hunger, R.; Jaegermann, W.; Merson, A.; Shapira, Y.; Pettenkofer, C.; Rappich, J. *J. Phys. Chem. B* **2006**, *110*, 15432–15441.
- Cotal, H.; Fetzer, C.; Boisvert, J.; Kinsey, G.; King, R.; Hebert, P.; Yoon, H.; Karam, N. *Energy Environ. Sci.* **2009**, *2*, 174–192.
- Lao, C.; Li, Y.; Wong, C. P.; Wang, Z. L. *Nano Lett.* **2007**, *7*, 1323–1328.
- McKone, J. R.; Warren, E. L.; Bierman, M. J.; Boettcher, S. W.; Brunschwig, B. S.; Lewis, N. S.; Gray, H. B. *Energy Environ. Sci.* **2011**, *4*, 3573–3583.